

Radiative symmetry breaking in a gauged Zee-Babu model and its gravitational wave imprints

Indra Kumar Banerjee,^{a,*} Nabarun Chakrabarty,^{b,†} Ujjal Kumar Dey^{a,‡}

^a*Department of Physical Sciences, Indian Institute of Science Education and Research Berhampur, Ganjam, Odisha 760003, India*

^b*Department of Physics, Siksha Bhavana, Visva-Bharati, Santiniketan, West Bengal 731235, India*

Abstract

We construct a classically scale invariant version of the Zee-Babu model governed by an $U(1)_{B-L}$ gauge symmetry wherein three right handed neutrinos with identical gauge charges are present. A \mathbb{Z}_2 symmetry is additionally imposed such that the lightest right handed neutrino becomes a dark matter candidate. A spontaneous breakdown of the $U(1)_{B-L}$ gauge group is triggered radiatively through renormalisation group effects and the dimensionful parameters thus emerging are proportional to the corresponding breaking scale v_{BL} . We demonstrate in this study how the same v_{BL} controls the dynamics of neutrino mass generation, lepton flavour violation and dark matter phenomenology. It is revealed that the scenario can simultaneously accommodate the observed neutrino masses and mixings, an appropriately low lepton flavour violation and the observed dark matter relic density for $10 \text{ TeV} \lesssim v_{BL} \lesssim 55 \text{ TeV}$. In addition, the very radiative nature of the set-up signals a strong first order phase transition in the presence of a non-zero temperature. Stochastic gravitational waves stemming from this phase transition are within the reach of detectors such as LISA and BBO. The scenario therefore emerges as a concrete platform to test classical scale invariance that is tied to neutrino masses and dark matter, through gravitational waves.

^{*}indrab@iiserbpr.ac.in

[†]nabarun.chakrabarty@visva-bharati.ac.in

[‡]ujjal@iiserbpr.ac.in

Contents

1	Introduction	2
2	Scale-invariant Zee-Babu framework and radiative symmetry breaking	3
3	Neutrino, lepton flavour violation, and collider constraints	7
4	Dark matter phenomenology	10
5	First order phase transition and gravitational waves	11
6	Conclusions	17

1 Introduction

Despite the success of the Standard Model (SM), several unresolved issues on both theoretical and experimental fronts keep advocating for additional dynamics. One such area is the SM’s inability to predict non-zero masses for neutrinos and the observed pattern of neutrino-mixing. Massive neutrinos provide concrete hints of physics beyond the SM (BSM) and many theoretical possibilities have been proposed to account for the lightness of neutrinos (see [1–4] for some reviews). An elegant framework to generate non-zero masses is the Zee-Babu model [5–7] that features a singly charged scalar and a doubly charged scalar over and above the SM fields. Neutrino masses are generated at the two-loop level and are proportional to the Yukawa couplings of the new scalars and inversely proportional to the square of their masses. For fixed Yukawas, the two-loop dynamics dictates that the additional scalars are lighter than what they would be in a typical tree-level neutrino mass framework, thereby bringing down their masses within the purview of present and future colliders.

On another front, around 27% of the total mass energy budget of the universe is found to consist of an hitherto unobserved non-luminous, non-baryonic matter called dark matter (DM) [8–10]. Denoting the corresponding density parameter as Ω_{DM} , one has [11]

$$\Omega_{\text{DM}}h^2 = 0.120 \pm 0.001, \quad (1)$$

where $h = \text{Hubble parameter}/(100 \text{ km/s/Mpc})$. If the dark matter is hypothesized to be an elementary particle, then there is no candidate for the same in the SM. While a host of particle DM models with different DM production mechanisms exist in the literature, the Weakly Interacting Massive Particle (WIMP) is the most widely studied (some reviews are [12–14]). Here, the interaction strengths involving the DM and bath particles are in the *weak* ballpark as a result of which DM *freezes-out* from thermal equilibrium thereby generating the relic density. However, the very fact that DM interaction strengths are sizeable has cornered most minimal WIMP scenarios in view of the null results from direct detection experiments such as XENON-1T [15], PANDA-X [16] and LUX-ZEPELIN [17] more so for a DM mass in the [10 GeV, 1 TeV] range. The only shot at salvaging such models is when the dark matter mass is outside the aforesaid range.

In recent years, first-order phase transitions (FOPTs) in scalar extensions of the Standard Model have emerged as a promising source of stochastic gravitational waves (GWs) potentially observable by forthcoming space-based interferometers. While the presence of additional bosonic degrees of freedom can accommodate a strong FOPT, the transition dynamics can be significantly enriched in scenarios where symmetry breaking occurs radiatively, leading to the dynamical generation of a new scale. In this context, the possibility that such a dynamically generated scale is directly correlated with the neutrino mass scale is particularly intriguing, and the cosmological implications of this connection remain comparatively unexplored.

Motivated by these considerations, we construct a classically scale-invariant extension of the well known Zee-Babu model [5–7] by endowing it with an $U(1)_{B-L}$ gauge symmetry. Anomaly cancellation in this framework requires the inclusion of three right-handed neutrinos (RHNs), which we take to be odd under a discrete \mathbb{Z}_2 symmetry thereby rendering the lightest RHN a potential dark matter (DM) candidate. The $U(1)_{B-L}$ is broken radiatively when the renormalisation group (RG)-improved scalar potential develops a minimum at a scale v_{BL} . An immediate observation is that the crucial scalar trilinear interaction responsible for neutrino mass in the minimal Zee-Babu case is now generated from a quartic interaction after symmetry breaking. Since the same v_{BL} controls the size of neutrino masses while being subject to lower bounds from collider searches, the model naturally leads to a nontrivial interplay between neutrino phenomenology and symmetry-breaking dynamics. The same connection is also expected in the case of the $\ell_i \rightarrow \ell_j \ell_k \ell_l$ and $\ell_i \rightarrow \ell_j \gamma$ lepton flavor violating (LFV) processes mediated by the Zee-Babu scalars. In addition, the presence of the $U(1)_{B-L}$ sector opens up new annihilation channels for the dark matter candidate, thereby modifying the relic abundance relative to the minimal Zee–Babu scenario. In addition, incorporating $T \neq 0$ corrections in the RG-improved potential can give rise to strong FOPTs thereby providing a source of GWs. In all, we aim to see if the observed pattern of neutrino masses, DM relic density, an appropriately low LFV and detectable GWs can be simultaneously accommodated by a judicious choice of the symmetry breaking scale v_{BL} in the otherwise scale invariant scenario. Some aspects of the $U(1)_{B-L}$ extension in the context of dark matter, neutrino, gravitational waves and allied phenomena are discussed in [18–21].

This article is organised as follows. We introduce the scale-invariant Zee-Babu framework in section 2 and discuss the radiative symmetry breaking. Section 3 details a fitting of neutrino data in this framework. The same section also translates bounds coming from LFV and colliders to constraints on the model parameters. The DM phenomenology is outlined in section 4. FOPT and production of GWs is discussed in section 5 and we conclude in section 6. Important formulae are relegated to the Appendix.

2 Scale-invariant Zee-Babu framework and radiative symmetry breaking

We first describe the minimal Zee-Babu model in a nutshell in this section. Over and above the SM fields, this model employs two scalars h^+ and k^{++} whose SM quantum numbers are given below.

Field	$SU(3)_c$	$SU(2)_L$	$U(1)_Y$
k^{++}	1	1	2
h^+	1	1	1

The scalar potential is given by,

$$V_{\text{tree}} = \mu_H^2 H^\dagger H + \mu_h^2 |h^+|^2 + \mu_k^2 |k^{++}|^2 + (\mu_3 k^{++} h^- h^- + \text{h.c.}) + \lambda_H (H^\dagger H)^2 + \lambda_h (h^+ h^-)^2 + \lambda_k (k^{++} k^{--})^2 + \lambda_1 (H^\dagger H) (h^+ h^-) + \lambda_2 (H^\dagger H) (k^{++} k^{--}) + \lambda_6 (h^+ h^-) (k^{++} k^{--}), \quad (2)$$

where $H = \begin{pmatrix} G^+ \\ \frac{1}{\sqrt{2}}(v + h_0 + iG_0) \end{pmatrix}$ is the SM-like $SU(2)_L$ Higgs doublet and $v = 246$ GeV is the vacuum expectation value (VEV). Next, the Yukawa interactions involving the BSM fields are,

$$-\mathcal{L}_Y^{h,k} = \left[\sum_{i,j=1,2,3} y_1^{ij} \overline{L_{Li}^c} L_{Lj} h^+ + \sum_{i,j=1,2,3} y_2^{ij} \overline{l_{Ri}^c} l_{Rj} k^{++} + \text{h.c.} \right]. \quad (3)$$

Assuming the scenario is governed by a global $U(1)_L$, the scalars h^+ and k^{++} each carry a charge = +2 under the same. It then follows that the trilinear term in the scalar potential violates $U(1)_L$ by 2 unit, opening up a possibility of generation of Majorana masses for the neutrinos. In the context of the Zee-Babu model, this famously occurs through a two-loop amplitude. The Zee-Babu model is subject to constraints from colliders, non-standard neutrino interactions [22, 23] and lepton flavor violation (LFV). Studies on the stability of the electroweak vacuum are performed in [24, 25] while radiative corrections to couplings are computed in [26]. Collider signatures of the Zee-Babu model have been investigated in [27–36]. Electroweak baryogenesis and GWs are looked at in [37]. Some interesting extensions of this model are [38–42].

The scalar trilinear operator $k^{++} h^- h^-$ is thus crucial from the perspective of neutrino mass generation in the Zee-Babu set-up. We therefore introduce an additional scalar S and explore the possibility that the aforementioned trilinear operator is generated from a quartic operator via $S k^{++} h^- h^- \rightarrow \langle S \rangle k^{++} h^- h^-$, where $\langle S \rangle$ denotes the VEV of S . This warrants a classical scale invariant approach¹. Moreover, we stipulate that S, h^+, k^{++} each carry +2 units of charge under an $U(1)_{B-L}$ gauge symmetry such that the parent $S k^{++} h^- h^-$ operator stays invariant under the same. The upshot of such a construct is two-fold at this stage. First, the breaking of the $U(1)_L$ is seen as a consequence of a spontaneous breakdown of the $U(1)_{B-L}$. Secondly, the invoked classical scale invariance renders the model economical in terms of parameter count and theoretically attractive.

A gauged $U(1)_{B-L}$ necessitates introduction of three right handed neutrinos (RHNs) $N_{1,2,3}$ to ensure cancellation of gauge anomalies. A \mathbb{Z}_2 symmetry is invoked and N_i are assigned a negative \mathbb{Z}_2 charge so that the lightest of them becomes a potential DM candidate. In all, the charges of all fields under the $SU(3)_c \times SU(2)_L \times U(1)_Y \times U(1)_{B-L} \times \mathbb{Z}_2$ symmetry² are listed below in table 1. In the presence of the additional field S , the scalar potential at the tree level can be extended from Eq. (2) and is given by,

$$V_{\text{tree}} = \lambda_H (H^\dagger H)^2 + \lambda_h (h^+ h^-)^2 + \lambda_k (k^{++} k^{--})^2 + \lambda_S (S^* S)^2 + \lambda_1 (H^\dagger H) (h^+ h^-) + \lambda_2 (H^\dagger H) (k^{++} k^{--}) + \lambda_3 (H^\dagger H) (S^* S) + \lambda_4 (h^+ h^-) (S^* S) + \lambda_5 (k^{++} k^{--}) (S^* S) + \lambda_6 (h^+ h^-) (k^{++} k^{--}) + \left[\lambda_7 S k^{++} h^- h^- + \text{h.c.} \right]. \quad (4)$$

¹Classical scale-invariance in neutrino mass models was first studied in [43].

²An $U(1)_{B-L}$ extension of the Zee-Babu model was studied in [44]. However, the framework was not classically scale invariant and featured a larger field content.

Field	$SU(3)_c$	$SU(2)_L$	$U(1)_Y$	$U(1)_{B-L}$	\mathbb{Z}_2
Q_L	3	2	1/6	1/3	+
L_L	1	2	-1/2	-1	+
u_R, d_R	3	1	2/3, -1/3	1/3	+
l_R	1	1	-1	-1	+
$N_{1,2,3}$	1	1	1	-1	-
H	1	2	1/2	0	+
k^{++}	1	1	2	2	+
h^+	1	1	1	2	+
S	1	1	0	2	+

Table 1: Quantum numbers of the various fields under the gauge and \mathbb{Z}_2 symmetry

The multiplets H and S are expressed as

$$H = \begin{pmatrix} G^+ \\ \frac{1}{\sqrt{2}}(h_0 + iG_0) \end{pmatrix}, \quad S = \frac{1}{\sqrt{2}}(s_0 + ia_0). \quad (5)$$

The following Yukawa term can be added with the introduction of the RHNs.

$$-\mathcal{L}_Y = \left[\sum_{ij=1,2,3} (Y_S)_{ij} \bar{N}_i^c N_j S + \text{h.c.} \right]. \quad (6)$$

The Yukawa coupling matrix Y_S can be chosen to be $\text{diag}(y_{S1}, y_{S2}, y_{S3})$ and real without any loss of generality.

Next, we explore possible radiative breaking of the $U(1)_{B-L}$ symmetry in the direction of S . The RG-improved potential for $S = \frac{\phi}{\sqrt{2}}$ reads

$$V_{\text{RG}}(\phi) = \frac{1}{4} \lambda_S(t) \phi^4. \quad (7)$$

In Eq. (7), ϕ refers to the background field and $t = \log(\phi/\mu)$ with μ denoting the dimensional regularisation scale. The quantity $\lambda_S(t)$ refers to the quartic coupling λ_S at the corresponding value of ϕ and can be obtained by solving the RG equations for this model. Thus, RG equations at a given loop order (say) introduces radiative effects to $V_{\text{RG}}(\phi)$ at that loop order. The dominant contribution typically comes at the one-loop level for the parameter ranges of our interest and therefore we adhere to it accordingly. A complete list of one-loop RG equations for this framework is given in the Appendix. We denote $\langle S \rangle$ by $\frac{1}{\sqrt{2}}v_{BL}$ in this work and demand that $V_{\text{RG}}(\phi)$ has a minimum at $\phi = v_{BL}$. In other words,

$$\frac{dV_{\text{RG}}}{d\phi} \Big|_{\phi=v_{BL}} = 0, \quad (8)$$

Choosing $\mu = v_{BL}$ leads to

$$4\lambda_S(0) + \beta_{\lambda_S}(0) = 0, \quad (9)$$

i.e.,

$$64\pi^2\lambda_S(0) + 20\lambda_S^2(0) + 2\lambda_3^2(0) + \lambda_4^2(0) + \lambda_5^2(0) - 48\lambda_S(0)g_{BL}^2(0) + 8\lambda_S(0)\text{Tr}[Y_S^\dagger Y_S](0) + 96g_{BL}^2(0) - \text{Tr}[Y_S^\dagger Y_S Y_S^\dagger Y_S](0) = 0. \quad (10)$$

One numerically solves for $\lambda_S(0)$ from Eq. (10) for given values of the other couplings at $t = 0$. The one-loop β -functions for this model are given in the Appendix. Of all model couplings, the RG-improved potential $V_{RG}(\phi)$ is more sensitive to the ones entering β_{λ_S} . To illustrate the behaviour of the RG-improved potential, we fix $\lambda_1(0) = \lambda_2(0) = \lambda_3(0) = \lambda_6(0) = 0.01$, $\lambda_7(0) = 0.7$ and plot $V_{RG}(\phi)$ versus ϕ in Fig. 1 for the shown values of the other couplings. The following is then inferred.

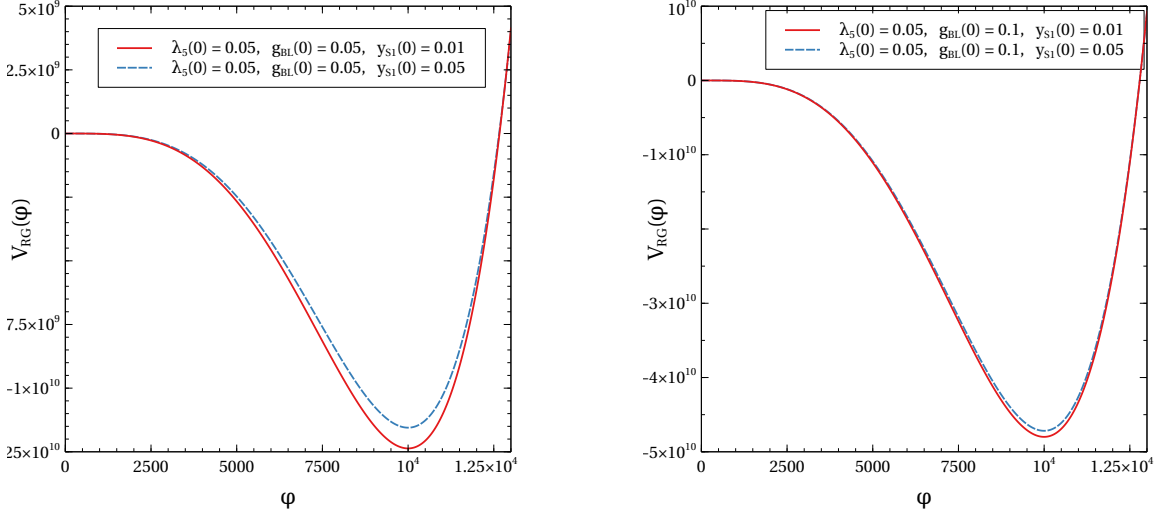


Figure 1: Variation of $V_{RG}(\phi)$ versus ϕ for $v_{BL} = 10^4$ GeV and for the choices of $\lambda_5(0)$, $g_{BL}(0)$ and $y_1(0)$ mentioned in the legends. We have further taken $y_{S2}(0) = y_{S3}(0) = 2y_{S1}(0)$ in this case.

First, $\lambda_S(0)$ must be negative for $V_{RG}(\phi)$ to have a minima at $\phi = v_{BL}$. This accordingly constrains the other couplings at $t = 0$ through Eq. (10). Given the presence of both bosonic as well as fermionic terms in β_{λ_S} , Choosing higher values for the former (latter) at $t = 0$ accordingly leads to a higher (lower) value of $|\lambda_S(0)|$. Moreover, the larger (smaller) is $|\lambda_S(0)|$, the deeper (shallow) is the minima. These inferences are indeed corroborated by Fig. 1.

Further, electroweak symmetry breaking (EWSB) occurs when h_0 picks up a VEV following which the $SU(2)_L \times U(1)_Y \times U(1)_{B-L} \rightarrow U(1)_Q$ breakdown is complete and therefore $h_0 = v + h'_0$, $s_0 = v_{BL} + s'_0$. An h'_0 - s'_0 mixing arises and is controlled by $\lambda_3(0)$ leading to the mass eigenstates h, h_2 through,

$$\begin{pmatrix} h \\ h_2 \end{pmatrix} = \begin{pmatrix} \cos\theta & \sin\theta \\ -\sin\theta & \cos\theta \end{pmatrix} \begin{pmatrix} h'_0 \\ s'_0 \end{pmatrix}, \quad (11)$$

where θ is a mixing angle. Stipulating $v_{BL} \gg v$, $\lambda_3(0)v_{BL}^2 = -2\lambda_H(0)v^2$, $\lambda_H(0) = m_h^2/(2v^2)$ ensures a low mixing and an observed Higgs mass $m_h = 125$ GeV. We end this section by quoting below the masses for the BSM fields in terms of relevant couplings and VEVs,

$$m_{h^+}^2 = \frac{1}{2}(\lambda_1 v^2 + \lambda_4 v_{BL}^2), \quad (12a)$$

$$m_{k^{++}}^2 = \frac{1}{2}(\lambda_2 v^2 + \lambda_5 v_{BL}^2), \quad (12b)$$

$$m_{Z_{BL}} = 2g_{BL}v_{BL}, \quad (12c)$$

$$m_{N_i} = \frac{1}{\sqrt{2}}y_{Si}v_{BL}. \quad (12d)$$

3 Neutrino, lepton flavour violation, and collider constraints

Neutrino masses are generated in this framework at two-loops in the usual Zee-Babu fashion with the trilinear parameter $\mu_3 = \lambda_7(0)v_{BL}$. The elements of the corresponding mass matrix are given by [45],

$$(m_\nu)_{ij} = \sum_{p,q=1,2,3} 16\lambda_7(0)v_{BL} y_1^{ip}m_p y_2^{pq}\mathcal{I}_{pq}m_q y_1^{qj}. \quad (13)$$

The function $\tilde{I}_{pq}(r)$ stemming from the two-loop integral can be approximated as,

$$\tilde{I}_{pq}(r) = \frac{\pi^2}{3(16\pi^2)^2} \frac{\delta_{pq}}{M^2} g(r), \quad (14)$$

with $M = \max(m_{h^+}, m_{k^{++}})$ and $g(r) = 1 + \frac{3}{\pi^2}(\ln^2(r) - 1)$ for $r > 1$ [45]. Eq. (13) can be expressed in the matrix form as,

$$m_\nu = Y_1^T f Y_1, \quad (15)$$

where $f_{ij} = 16\lambda_7(0)v_{BL}m_i m_j I_{ij} y_2^{ij}$. The Pontecorvo-Maki-Nakagawa-Sakata (PMNS) matrix U brings m_ν to a diagonal form through $\hat{m}_\nu = U^T m_\nu U$ with $\hat{m}_\nu = \text{diag}(m_{\nu_1}, m_{\nu_2}, m_{\nu_3})$. Since $\mu_3, m_{h^+}, m_{k^{++}} \sim v_{BL}$ in this scale invariant set-up, the neutrino mass scale is approximately given by,

$$m_\nu \sim \left(\frac{1}{16\pi^2}\right)^2 \left(\frac{\lambda_7 a^2 b}{\lambda_5}\right) \left(\frac{m_{\text{lepton}}^2}{v_{BL}}\right). \quad (16)$$

In Eq. (16), a and b are used to denote the orders of magnitude of y_1^{ij} and y_2^{ij} . The light neutrino mass scale is therefore dynamically generated from v_{BL} . This is a crucial difference from the minimal Zee-Babu model in which case μ_3 and the Zee-Babu masses are *a priori* uncorrelated. Having said so, we now look to fit the neutrino data more accurately in this scenario. Employing the Casas-Ibarra parameterisation [46] for Majorana neutrino masses, one writes

$$Y_1 = V^* f^{-1/2} R (\hat{m}_\nu)^{1/2} U^\dagger, \quad (17)$$

where V diagonalises f through $V^\dagger f V = \hat{f}$. One notes that $V = I_{3 \times 3}$ here since f is diagonal. More specifically, for $m_{h^{++}} > m_{k^+}$,

$$f \sim \frac{32}{(16\pi^2)^2} \left(\frac{\lambda_7}{\lambda_5}\right) \left(\frac{1}{v_{BL}}\right) \text{diag}(y_2^{ee} m_e^2, y_2^{\mu\mu} m_\mu^2, y_2^{\tau\tau} m_\tau^2). \quad (18)$$

In addition, R is an arbitrary 3×3 complex orthogonal matrix. The PMNS matrix has the form

$$U = \begin{pmatrix} c_{12}c_{13} & s_{12}c_{13} & s_{13}e^{-i\delta} \\ -s_{12}c_{23} - c_{12}s_{23}s_{13}e^{i\delta} & c_{12}c_{23} - s_{12}s_{23}s_{13}e^{i\delta} & s_{23}c_{13} \\ s_{12}s_{23} - c_{12}c_{23}s_{13}e^{i\delta} & -c_{12}s_{23} - s_{12}c_{23}s_{13}e^{i\delta} & c_{23}c_{13} \end{pmatrix} \quad (19)$$

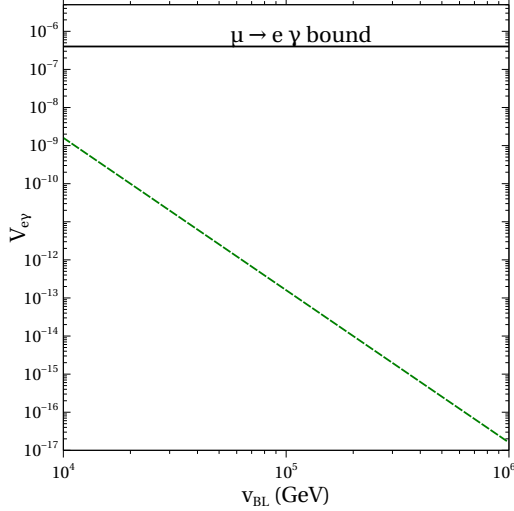


Figure 2: Lepton flavour violation constraints in terms of the dimensionless parameter $V_{e\gamma}$ (see Eq. (21a)).

with the shorthand $s_{ij}(c_{ij}) = \sin\theta_{ij}(\cos\theta_{ij})$. Choosing Normal Hierarchy (NH), we take the neutrino oscillation parameters as, $\theta_{12} = 33.68^\circ$, $\theta_{23} = 48.5^\circ$, $\theta_{13} = 8.52^\circ$, $\delta_{CP} = 177^\circ$, $\Delta m_{21}^2 = 7.5 \times 10^{-5}$ eV 2 , $\Delta m_{31}^2 = 2.5 \times 10^{-3}$ eV 2 from the NuFit-6.0 analysis [47].

The Zee-Babu scalars h^+ and k^{++} mediate $\ell_i \rightarrow \ell_j \ell_k \bar{\ell}_l$ and $\ell_i \rightarrow \ell_j \gamma$ LFV processes. Upper bounds on the corresponding branching ratios therefore accordingly constrain the size of y_1^{ij} and y_2^{ij} . We refer to [48] for a list of such bounds and refrain from discussing this here in detail for brevity. For instance, the most stringent limits come from $\mu \rightarrow ee\bar{e}$ [49] and $\mu \rightarrow e\gamma$ [50], and, are seen to lead to [48],

$$|y_2^{ee}(y_2^{e\mu})^*| < 2.3 \times 10^{-5} \left(m_{k^{++}}/\text{TeV} \right)^2, \quad (20a)$$

$$r^2 |(y_1^{e\tau})^* y_1^{\mu\tau}|^2 + 16 |(y_2^{ee})^* y_2^{e\mu} + (y_2^{e\mu})^* y_2^{\mu\mu} + (y_2^{e\tau})^* y_2^{\mu\tau}|^2 < 1.6 \times 10^{-6} (m_{k^{++}}/\text{TeV})^4. \quad (20b)$$

In this study, the matrix y_1 is reconstructed for a fixed y_2 and R using Eq. (17). We next discuss possible constraints from colliders. A non-observation of a Z_{BL} gauge boson at LEP-II enforces $m_{Z_{BL}}/g_{BL} \gtrsim 7.1$ TeV [51] in this framework which ultimately translates to $v_{BL} \gtrsim 3.55$ TeV. We adopt a more conservative approach and adhere to $v_{BL} \geq 10$ TeV in view of tighter bounds in the future. A LEP exclusion limit also reads $m_{h^+} > 100$ GeV leading to $v_{BL} \gtrsim \frac{142}{\sqrt{\lambda_4}}$ GeV for λ_4 and λ_1 of comparable magnitudes. A more stringent exclusion bound of $m_{k^{++}} > 600$ GeV applies to this setup from the non-observation of the $k^{++} \rightarrow \ell^+ \ell^+$ decay mode at the LHC translating to $v_{BL} \gtrsim \frac{142}{\sqrt{\lambda_5}}$ GeV for λ_5 and λ_2 of comparable magnitudes.

The bounds stated in Eqs. (20a)-(20b) in the present scale-invariant framework can be interpreted on bounds on two dimensionless variables V_{3e} and $V_{e\gamma}$. That is,

$$V_{e\gamma} \equiv \frac{|y_2^{ee}(y_2^{e\mu})^*|}{\lambda_5} \frac{1}{(v_{BL}/\text{TeV})^2} < 1.15 \times 10^{-5}, \quad (21a)$$

$$V_{3e} \equiv \frac{r^2 |(y_1^{e\tau})^* y_1^{\mu\tau}|^2 + 16 |(y_2^{ee})^* y_2^{e\mu} + (y_2^{e\mu})^* y_2^{\mu\mu} + (y_2^{e\tau})^* y_2^{\mu\tau}|^2}{\lambda_5^2} \frac{1}{(v_{BL}/\text{TeV})^4} < 4 \times 10^{-7}. \quad (21b)$$

We observe that choosing $|y_2^{ij}| \gtrsim 10^{-2}$ for $\lambda_5 \sim 0.1$ and $v_{BL} > 10$ TeV suffices to bypass all $l_i \rightarrow l_j \gamma$ bounds. Therefore we choose $Y_2 = \begin{pmatrix} 1 & 1 & 1 \\ 1 & 1 & 1 \\ 1 & 1 & 1 \end{pmatrix} \times 10^{-2}$, $\lambda_4 = 0.1$, $\lambda_5 = 0.3$ and study the variation of $V_{e\gamma}$ in Fig. 2.

It is therefore inferred from Fig. 2 that the $v_{BL} \gtrsim 10$ TeV predicts LFV below the current limits while accounting for the observed neutrino masses and mixings.

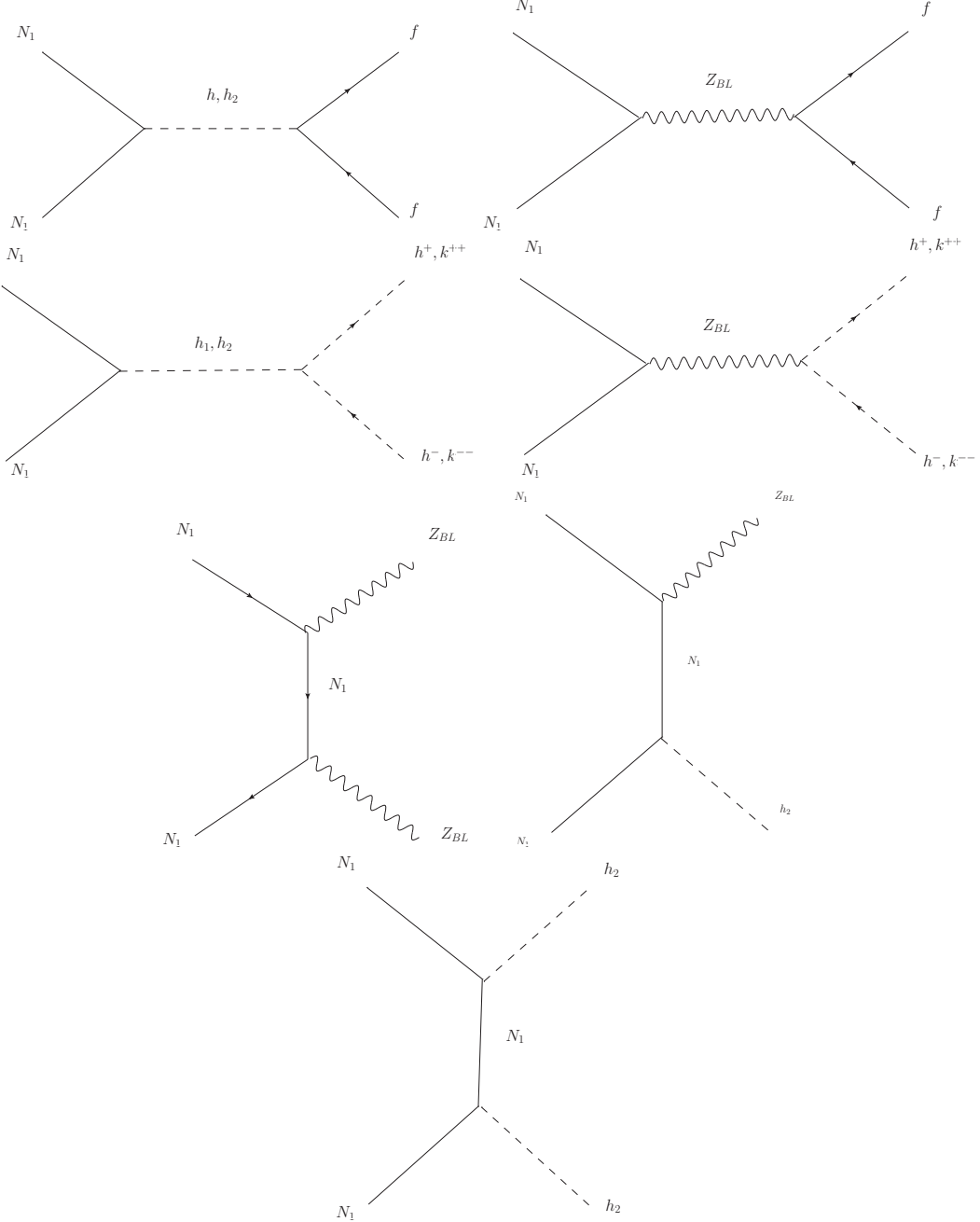


Figure 3: The DM annihilation channels in this model.

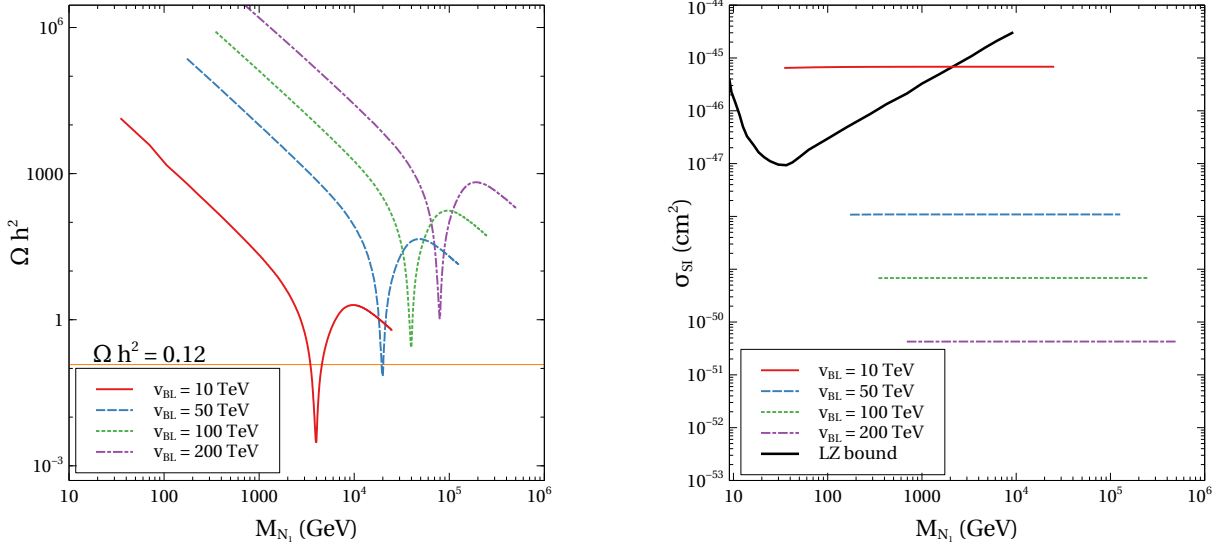


Figure 4: (Left) Variation of Ωh^2 with M_{N_1} for different values of v_{BL} . The values of the other model parameters are mentioned in the text. The horizontal line denotes the Planck central value. (Right) Dependence of spin-independent direct detection cross section on the M_{N_1} for different values of v_{BL} . The black solid curve represents the bound from LUX-ZEPELIN experiment.

4 Dark matter phenomenology

The dark matter phenomenology in the present framework is qualitatively similar to that of minimal $U(1)_{B-L}$ case. We choose N_1 as the DM candidate by ensuring that $y_{S1} < y_{S2}, y_{S3}$. The DM relic density is dictated by the $N_1 \bar{N}_1$ annihilations to the particles in the thermal bath as shown in Fig. 3.

It is pointed out that $N_1 \bar{N}_1 \rightarrow h^+ h^-$, $k^{++} k^{--}$ annihilations can possibly occur in this framework that are absent in the minimal $U(1)_{B-L}$ case. We implement the model in LanHEP [52]. A compatible output is then fed into the publicly available tool `micrOMEGAs` [53] to compute the relic density of N_1 .

We work in a rather conservative $v_{BL} > 10$ TeV region in this study in view of the non-observation bound from LHC. The left panel of Fig. 4 displays the variation of the relic density with the DM mass for $v_{BL} = 10$ TeV, 50 TeV, 100 TeV and 200 TeV. As for the values of the other model parameters, it must be noted that the annihilation cross sections have no or negligible dependence on the scalar couplings $\lambda_H, \lambda_h, \lambda_k, \lambda_1, \lambda_2, \lambda_6, \lambda_7$. Therefore we choose $\lambda_h(0) = \lambda_k(0) = \lambda_1(0) = \lambda_2(0) = \lambda_6(0) = \lambda_7(0) = 0.01$ ³. We also take $g_{BL}(0) = 0.4$ given that the annihilations are dominated by Z_{BL} -mediation and hence the dependence on the gauge coupling is also mild. Finally, we take $3\lambda_4(0) = \lambda_5(0) = 0.3$, $\lambda_S(0) = -3 \times 10^{-5}$ and vary $0.005 < y_{S1} < \sqrt{4\pi}$ while maintaining M_{N_1} to be the lightest RHN. Given the dominant Z_{BL} mediation, resonance dips are observed in Ωh^2 for $2M_{N_1} \simeq M_{Z_{BL}}$, that is, for $y_{S1}(0) \simeq \sqrt{2}g_{BL}(0)$. We also report an up to $\simeq 20\%$ contribution to the total annihilation cross section from the $h^+ h^-$, $k^{++} k^{--}$ final states. DM-nucleon scattering processes are triggered via t -channel mediation of Z_{BL} and are $\propto 1/v_{BL}^4$. Currently the most stringent bound on the spin-independent direct detection cross section comes from the LUX-ZEPELIN (LZ) experiment. The cross sections and the LZ bound are both shown in the right panel of Fig. 4. An inspection of both its

³The values of the independent parameters are assigned at the breaking scale v_{BL} in our scale-invariant approach.

panels suggests that stipulating that N_1 accounts entirely for the observed DM, and at the same time, predicts direct detection cross section below the latest bound implies that the symmetry breaking scale is bounded from both ends, i.e., $10 \text{ TeV} < v_{BL} < 55 \text{ TeV}$. Such a constraint on v_{BL} is thus stronger than what is obtained from LFV alone. This point is a key takeaway of our analysis as a result of which we obtain a window of v_{BL} to probe via GWs.

5 First order phase transition and gravitational waves

We first discuss of possibility of FOPT in the present set-up. The thermal potential reads,

$$V_T(\phi, T) = \sum_{b=h, G^0, G^+, h^+, k^{++}, S} n_b J_B \left(\frac{M_b^2(\phi)}{T^2} \right) + \sum_{f=N_1, N_2, N_3} n_f J_F \left(\frac{M_f^2(\phi)}{T^2} \right), \quad (22)$$

where, the various field-dependent masses in this framework are given by,

$$M_{h_0}^2(\phi) = M_{G_0}^2(\phi) = M_{G^+}^2(\phi) = \frac{\lambda_3}{2} \phi^2, \quad (23a)$$

$$M_{h^+}^2(\phi) = \frac{\lambda_4}{2} \phi^2, \quad M_{k^{++}}^2(\phi) = \frac{\lambda_5}{2} \phi^2, \quad (23b)$$

$$M_{s_0}^2(\phi) = \frac{3\lambda_S}{2} \phi^2, \quad M_{a_0}^2(\phi) = \frac{\lambda_S}{2} \phi^2, \quad (23c)$$

$$M_{Z_{BL}}^2(\phi) = 4g_{BL}^2 \phi^2, \quad M_{N_i}^2(\phi) = \frac{y_{Si}^2}{2} \phi^2. \quad (23d)$$

the degrees of freedom of the various bosons and fermions in the model are $n_h = n_{G^0} = n_S = 1$, $n_{G^+} = n_{h^+} = n_{k^{++}} = 2$, $n_{N_i} = -4$. The functions $J_{B,F}(x)$ are defined as

$$J_{B,F}(x) = \int_0^\infty dx y^2 \log \left[1 \mp e^{-\sqrt{y^2+x}} \right]. \quad (24)$$

We also perform resummation in order to incorporate infra-red (IR) effects. The Arnold-Espinosa technique is adopted in this work in which the following daisy term is added to the thermal potential [54],

$$V_{\text{Daisy}}(\phi, T) = -\frac{T}{12\pi} \sum_{b=h, G^0, G^+, h^+, k^{++}, S} n_b \left[M_b^3(\phi, T) - M_b^3(\phi) \right]. \quad (25)$$

In the above, $M_b^2(\phi, T) = M_b^2(\phi) + \Pi_b(T)$, with $\Pi_b(T)$ being the thermal correction to the mass of the b -th boson. One finds

$$\Pi_{h_0}(T) = \Pi_{G_0}(T) = \Pi_{G^+}(T) = \frac{1}{12} \left(\lambda_1 + \lambda_2 + \lambda_3 + 6\lambda_H + \frac{3}{4}(g')^2 + \frac{9}{4}g^2 + 3y_t^2 \right) T^2, \quad (26a)$$

$$\begin{aligned} \Pi_{h^+}(T) &= \frac{1}{12} \left(2\lambda_1 + \lambda_4 + \lambda_6 + 4\lambda_h + 3(g')^2 \right. \\ &\quad \left. + 12g_{BL}^2 + \text{Tr}(Y_1^\dagger Y_1) \right) T^2, \end{aligned} \quad (26b)$$

$$\Pi_{k^{++}}(T) = \frac{1}{12} \left(2\lambda_2 + \lambda_5 + \lambda_6 + 4\lambda_k + 12(g')^2 + 12g_{BL}^2 \right) T^2, \quad (26c)$$

$$\begin{aligned}\Pi_{s_0}(T) = \Pi_{a_0}(T) &= \frac{1}{12} \left(2\lambda_3 + \lambda_4 + \lambda_5 + 3\lambda_S \right. \\ &\quad \left. + 12g_{BL}^2 + \frac{1}{2} \text{Tr}(Y_2^\dagger Y_2) \right) T^2.\end{aligned}\quad (26d)$$

In addition, all couplings featuring in $V_T(\phi, T)$ and $V_{\text{Daisy}}(\phi, T)$ are determined at the energy scale ϕ through RG evolution. The total potential is given by $V_{\text{tot}}(\phi, T) = V_{\text{RG}}(\phi) + V_T(\phi, T) + V_{\text{Daisy}}(\phi, T)$. The thermal potential behaves as $\sim \phi^2 T^2$ for small field values implying that $\phi = 0$ is a minima at a nonzero temperature. In fact, $V_{\text{tot}}(\phi, T)$ is symmetric at high temperatures with a single minima at $\phi = 0$. While the zero temperature RG-improved potential tends to dynamically break the $U(1)_{B-L}$ at $\phi = v_{BL}$, a symmetry-restoring effect comes from the $T \neq 0$ corrections leading to an interesting interplay. Therefore, $V_{\text{tot}}(\phi, T)$ develops an inflection point at a given temperature. As further temperature lowers, a new minima ($\phi_{\min}(T)$) appears thereby opening up the possibility of tunnelling. The tunnelling probability per unit 4-volume is given by [55],

$$\Gamma(T) \sim T^4 \left(\frac{S_E}{2\pi T} \right)^{3/2} e^{-\frac{S_E}{T}}. \quad (27)$$

Here, S_E is the classical euclidean ‘‘bounce’’ action in 3-dimensions calculated as

$$S_E = 4\pi \int_0^\infty dr r^2 \left[\frac{1}{2} \left(\frac{d\phi}{dr} \right)^2 + V_{\text{total}}(\phi, T) \right]. \quad (28)$$

The scalar field ϕ is derived by solving the classical field equation,

$$\frac{d^2\phi}{dr^2} + \frac{2}{r} \frac{d\phi}{dr} - \frac{\partial V_{\text{total}}}{\partial \phi} = 0. \quad (29)$$

A critical temperature T_c is identified through

$$V_{\text{tot}}(0, T_c) = V_{\text{tot}}(\phi_{\min}(T_c), T_c), \quad (30)$$

An FOPT is deemed *strong* if $\phi_{\min}(T_c)/T_c > 1$ [56, 57]. The bubble picture can be invoked to understand FOPT in analogy with the liquid-gas phase transition. In a sea of the false vacuum, it can be thought to be populated by bubbles containing the true vacuum. The bubbles grow in size as tunnelling progresses. At the nucleation temperature T_n , there is ~ 1 bubble per unit Hubble volume [58], i.e., $\Gamma(T_n) = H^4(T_n)$. The nucleation temperature can be computed using [58–60],

$$\frac{S_E(T_n)}{T_n} = 140. \quad (31)$$

In order to test the strength of FOPTs in the present framework, we choose the following benchmark points shown in Table 2. The values of the other parameters are fixed as,

$$\lambda_4(0) = 0.1, \quad \lambda_5(0) = 0.3, \quad \lambda_7(0) = 0.5, \quad Y_2(0) = \begin{pmatrix} 1 & 1 & 1 \\ 1 & 1 & 1 \\ 1 & 1 & 1 \end{pmatrix} \times 10^{-2}, \quad (32a)$$

$$\lambda_1(0) = \lambda_2(0) = \lambda_6(0) = 0.01. \quad (32b)$$

The benchmarks are characterised by $\mathcal{O}(0.1)$ values for the couplings that involve the scalar S . The values taken for the various parameters are consistent with neutrino data as well as bounds from

Benchmark	v_{BL} (TeV)	$g_{BL}(0)$	$\{y_{S1}(0), y_{S2}(0), y_{S3}(0)\}$	$Y_1(0)$
BP1	16.2	0.49	$\{0.62, 0.70, 0.70\}$	$\begin{pmatrix} 0 & 0 & 0 \\ 0.224 & 0.249 - 0.007i & -0.239 - 0.006i \\ -0.008 - 0.002i & 0.043 & 0.038 \end{pmatrix}$
BP2	22.0	0.54	$\{0.70, 0.76, 0.76\}$	$\begin{pmatrix} 0 & 0 & 0 \\ 0.261 & 0.291 - 0.008i & -0.278 - 0.007i \\ -0.009 - 0.0029i & 0.051 & 0.044 \end{pmatrix}$
BP3	40.0	0.52	$\{0.72, 0.77, 0.77\}$	$\begin{pmatrix} 0 & 0 & 0 \\ 0.352 & 0.392 - 0.011i & -0.375 - 0.010i \\ -0.013 - 0.004i & 0.069 & 0.059 \end{pmatrix}$
BP4	50.0	0.51	$\{0.72, 0.80, 0.80\}$	$\begin{pmatrix} 0 & 0 & 0 \\ 0.394 & 0.438 - 0.01i & -0.420 - 0.01i \\ -0.014 - 0.004i & 0.077 & 0.066 \end{pmatrix}$

Table 2: Benchmark points used in the numerical analysis.

LFV and colliders. They are also compatible with the observed DM relic density and the LZ bound on direct detection cross sections as can be read from Table 3. We add that we have handled the $J_{B/F}(x)$ functions numerically and refrained from taking simplifying high- T expansions of the same. In addition, $S_E(T)$, T_n are computed by fitting $V_{\text{tot}}(\phi, T)$ to an analytical form following Ref. [61].

The thermal potential profiles at $T = T_c, T_n$ for the chosen benchmarks is shown in Fig. 5. One inspects $\phi_{\min}(T_c)/T_c > 1$ for all BP1-4 implying that the FOPT is *strong* and this can be attributed to classical scale invariance. More importantly, the strength of the FOPT is mainly dictated by primarily the $g_{BL}(0)$ and the Yukawa couplings, i.e., as the $g_{BL}(0)$ increases the FOPT becomes weaker (see BP1 and BP4); along with that, for sufficiently large values of $g_{BL}(0)$, as the ratio $g_{BL}(0)/\max\{y_{S1}(0), y_{S2}(0), y_{S3}(0)\}$ decreases, the strength decreases (see BP2 and BP4). One also inspects that the ratio $T_c/T_n \in (2.75, 3.3)$ for all the BPs. A T_n significantly lower than T_c implies that the phase transition is appropriately delayed.

Before going into the discussion of the gravitational waves due to the FOPT, we define two very important quantities that not only provide us a quantification of the FOPT property, but are linked directly to the estimation of the gravitational wave spectra. The first one signifies the apparent strength of the FOPT and can be expressed as,

$$\alpha = \frac{1}{\rho_{\text{rad}}(T_n)} \left[\Delta V_{\text{tot}} - \frac{T}{4} \frac{d}{dT} (\Delta V_{\text{tot}}) \right]_{T=T_n}, \quad (33)$$

where $\Delta V_{\text{tot}} = V_{\text{tot}}|_{\phi=\phi_f} - V_{\text{tot}}|_{\phi=\phi_t}$, $\rho_{\text{rad}}(T) = \pi^2 g_* T^4 / 30$ and $\phi_{f(t)}$ is the value of the field at the false (true) vacuum. The other important quantity gives us an estimate of the inverse duration of the FOPT and can be expressed as,

$$\beta/H \approx T_n \left[\frac{d}{dT} \left(\frac{S_3}{T} \right) \right]_{T=T_n}. \quad (34)$$

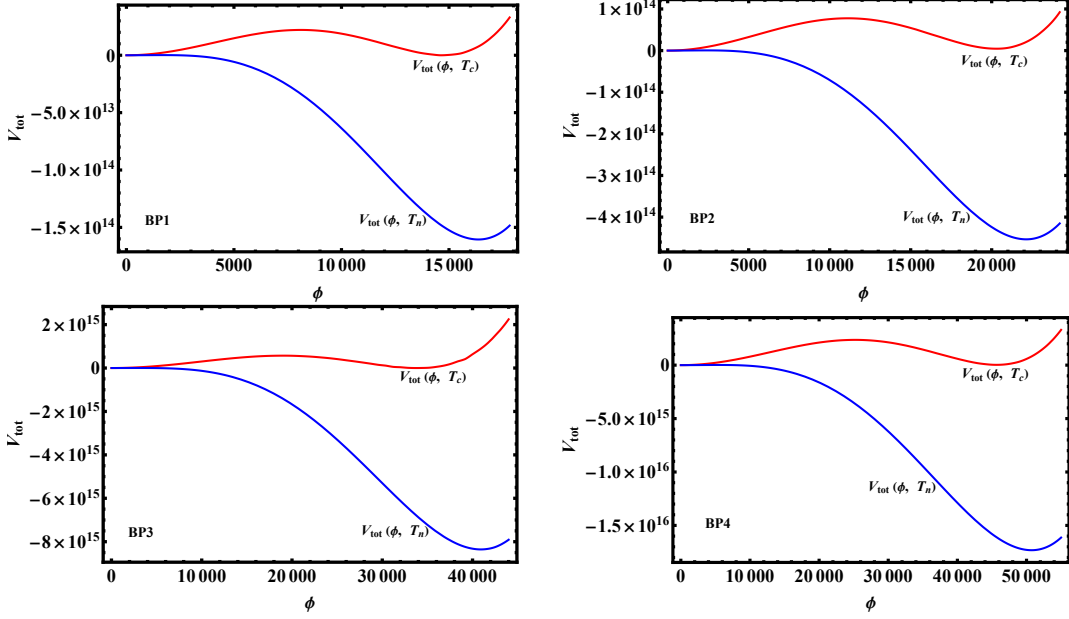


Figure 5: The shape of $V_{\text{tot}}(\phi, T)$ at $T = T_c, T_n$ for the four chosen benchmarks.

There are a few mechanisms through which gravitational waves can originate from FOPT, such as collision of bubble walls, the sound wave of the plasma, magnetohydrodynamic turbulence of the plasma, etc. The contribution of these sources depend on the distribution of the released latent heat, i.e., if more energy is released to the bubble walls then they tend to overcome the plasma friction and collide with each other making collision of bubble walls the dominant source whereas for weaker FOPTs more energy is released in the plasma and the friction inhibits the walls from colliding which makes the sound waves of the plasma the dominant source of gravitational waves. On this note, the most important aspect to determine is the dominant source of gravitational wave background for this case. In order to achieve that, we calculate the leading order plasma friction ΔP_{LO} , the bubble wall velocity v_w and the efficiency factor κ which signifies the energy distribution.

The leading order friction term can be expressed as [62, 63],

$$\Delta P_{\text{LO}} = \frac{\Delta m^2 T^2}{24}, \quad (35)$$

where

$$\Delta m^2 = \sum_i c_i N_i \Delta m_i^2, \quad (36)$$

with Δm_i^2 is the difference of the squared mass of the i -th particle species in true and false vacuum, N_i is the degree of freedom of the i -th particle species and $c_i = 1(1/2)$ for bosons (fermions). Now the plasma friction strength can be calculated as.

$$\alpha_\infty = \frac{\Delta P_{\text{LO}}}{\rho_R}, \quad (37)$$

where $\alpha = \alpha_\infty$ denotes the condition where the driving force on the vacuum wall is larger than the leading order friction. For $\alpha \gg \alpha_\infty$ leads to the creation of runaway bubbles and bubble wall collision

dominates, whereas for $\alpha \ll \alpha_\infty$ the bubble wall velocity is much less than the speed of light in most cases, and sound waves are the dominant source. However, we found that for the benchmark cases that we consider, α_∞ is marginally less than α , which leads to the scenario where in all cases, the gravitational waves due to both the bubble wall collision and the sound wave have to be considered.⁴

In order to calculate the contribution of the sound wave to the gravitational waves, we first lay the foundation with the calculation of the bubble wall velocity and the efficiency factor for the sound waves. To calculate the bubble wall velocity, we follow the prescription of Ref. [69], and use the approximate expression [70],

$$v_w = \begin{cases} \sqrt{\frac{\Delta V}{\alpha \rho_R}}, & \text{for } \sqrt{\frac{\Delta V}{\alpha \rho_R}} < v_J, \\ 1, & \text{for } \sqrt{\frac{\Delta V}{\alpha \rho_R}} > v_J, \end{cases} \quad (38)$$

where v_J is the Chapman-Jouguet velocity and can be expressed as [71–73],

$$v_J = \frac{1}{\sqrt{3}} \frac{1 + \sqrt{3\alpha^2 + 2\alpha}}{1 + \alpha}. \quad (39)$$

Using the above expression once the bubble wall velocity is obtained, one can then obtain the efficiency factor of the sound waves using the numerical fitting obtained in Ref. [73]. The efficiency factor depends on the wall velocity and can be expressed as,

$$\kappa_{sw} \approx \begin{cases} \frac{c_s^{11/5} \kappa_A \kappa_B}{(c_s^{11/5} - v_w^{11/5}) \kappa_B + v_w c_s^{6/5} \kappa_A} & \text{for } v_w \lesssim c_s, \\ \kappa_B + (v_w - c_s) \delta_\kappa + \frac{(v_w - c_s)^3}{(v_J - c_s)^3} [\kappa_C - \kappa_B - (v_J - c_s) \delta_\kappa] & \text{for } c_s < v_w < v_J, \\ \frac{(v_J - 1)^3 v_J^{5/2} v_w^{-5/2} \kappa_C \kappa_D}{[(v_J - 1)^3 - (v_w - 1)^3] v_J^{5/2} \kappa_C + (v_w - 1)^3 \kappa_D} & \text{for } v_w \gtrsim v_J, \end{cases} \quad (40)$$

where,

$$\kappa_A \approx v_w^{6/5} \frac{6.9\alpha}{1.36 - 0.037\sqrt{\alpha} + \alpha}, \quad (41)$$

$$\kappa_B \approx \frac{\alpha^{2/5}}{0.017 + (0.997 + \alpha)^{2/5}}, \quad (42)$$

$$\kappa_C \approx \frac{\sqrt{\alpha}}{0.135 + \sqrt{0.98 + \alpha}}, \quad (43)$$

$$\kappa_D \approx \frac{\alpha}{0.73 + 0.083\sqrt{\alpha} + \alpha}, \quad (44)$$

$$\delta_\kappa \approx -0.9 \log \frac{\sqrt{\alpha}}{1 + \sqrt{\alpha}}, \quad (45)$$

and $c_s = 1/\sqrt{3}$ is the speed of sound wave in plasma. It is to be noted that the first, second, and the third cases in Eq. (40) are sub-sonic deflagration, supersonic deflagration, and detonation respectively.

⁴It is to be noted that although several studies have investigated the GW spectra from the magneto-hydrodynamic turbulence of plasma surrounding the bubble wall [64–67], due to the existence of uncertainties in the spectral shape, we do not consider this source [68].

Benchmark	$\Omega_{N_1} h^2$	$\sigma_{SI}(\text{cm}^2)$	$T_c(\text{TeV})$	ϕ_c/T_c	$T_n(\text{TeV})$	v_w	κ_{sw}	α	β/H	α_∞
BP1	0.117	9.91×10^{-47}	7.8	1.91	2.73	0.752	0.455	0.141	198	0.082
BP2	0.111	2.91×10^{-47}	17.65	1.15	6.25	0.449	0.1938	0.079	189	0.034
BP3	0.113	2.66×10^{-48}	29.5	1.20	9.02	0.592	0.392	0.096	194	0.053
BP4	0.103	1.09×10^{-48}	25.6	1.79	9.27	0.713	0.482	0.126	208	0.075

Table 3: Parameters pertaining to DM, FOPT and GWs corresponding to the chosen benchmarks

Finally, the SGWB spectra due to sound waves can be expressed as [74–77],

$$\Omega_{sw} h^2 = 4.13 \times 10^{-7} (R_* H_*) \left(1 - \frac{1}{\sqrt{1 + 2\tau_{sw} H_*}} \right) \left(\frac{\kappa_{sw} \alpha}{1 + \alpha} \right)^2 \left(\frac{100}{g_*} \right)^{1/3} S_{sw}(f), \quad (46)$$

where, S_{sw} contains the information regarding the frequency dependence of the SGWB spectrum and can be expressed as,

$$S_{sw}(f) = \left(\frac{f}{f_{sw}} \right)^3 \left(\frac{4}{7} + \frac{3}{7} \left(\frac{f}{f_{sw}} \right)^2 \right)^{-7/2}, \quad (47)$$

the peak frequency of the spectrum is given by,

$$f_{sw} = 2.6 \times 10^{-5} (R_* H_*)^{-1} \left(\frac{T_n}{100 \text{ GeV}} \right) \left(\frac{g_*}{100} \right)^{1/6} \text{ Hz}, \quad (48)$$

and the other relevant quantities are defined as [63, 76, 78–80],

$$\tau_{sw} H_* = \frac{R_* H_*}{U_f}, \quad (49)$$

$$U_f = \sqrt{\frac{3}{4} \frac{\alpha}{1 + \alpha} \kappa_{sw}}, \quad (50)$$

$$R_* H_* = (8\pi)^{1/3} \max(v_w, c_s) \left(\frac{\beta}{H} \right)^{-1}. \quad (51)$$

On the other hand, to estimate the contribution of the bubble wall collision to the gravitational waves, one must first consider the efficiency factor of the energy released into the bubble walls. It has been shown that the efficiency factor can be expressed as [68],

$$\kappa_{coll} \approx \frac{\alpha - \alpha_\infty}{\alpha}. \quad (52)$$

Hence the SGWB spectra due to the bubble wall collision today can be expressed as [63, 81, 82],

$$\Omega_{coll} h^2 = 4 \times 10^{-7} (R_* H_*)^2 \left(\frac{100}{g_*} \right)^{1/3} \left(\frac{\kappa_{coll} \alpha}{1 + \alpha} \right)^2 S_{coll}(f), \quad (53)$$

where S_{coll} contains the information regarding the frequency dependence of the SGWB spectra and can be expressed as,

$$S_{coll}(f) = \left(\frac{f}{f_{coll}} \right)^3 \left(1 + 2 \left(\frac{f}{f_{coll}} \right)^{2.07} \right)^{-2.18}, \quad (54)$$

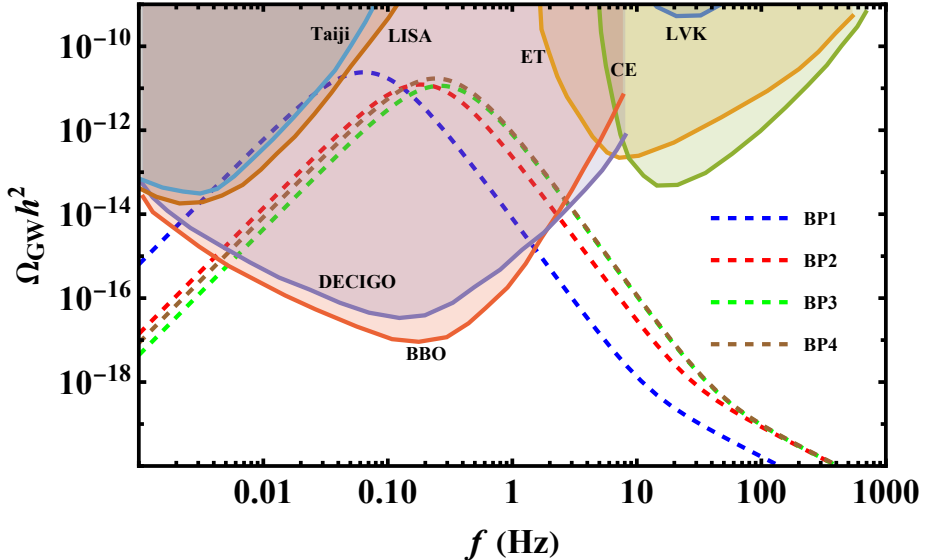


Figure 6: The gravitational wave signatures arising from the FOPT for the benchmark parameters considered. The projected sensitivity of current and upcoming GW experiments has been shown.

and the peak frequency of the spectrum can be expressed as

$$f_{\text{coll}} = 2.88 \times 10^{-6} \left(\frac{1}{v_w} \right) \left(\frac{\beta}{H} \right) \left(\frac{T_n}{100 \text{ GeV}} \right) \left(\frac{g_*}{100} \right)^{1/6} \text{ Hz.} \quad (55)$$

It is worth mentioning here that although the SGWB is calculated at the reheating temperature, in this case since $\alpha \ll 1$ for all the cases that we consider, the reheating temperature $T_{\text{reh}} \approx T_n$. Finally, the combined SGWB can be expressed as,

$$\Omega_{\text{GW}} h^2 = \Omega_{\text{sw}} h^2 + \Omega_{\text{coll}} h^2. \quad (56)$$

We show the variation of $\Omega_{\text{GW}} h^2$ versus the frequency f in Fig. 6. The sensitivities of different future space-based GW interferometers such as LISA [83], BBO [84], DECIGO [85], Taiji [86], ET [87], CE [88] and LVK (LIGO-Virgo-KAGRA) [89–91] are also shown in Fig. 6. The GW spectra for the chosen BPs peak in the frequency range $\mathcal{O}(0.01) - \mathcal{O}(0.1)$ Hz with the peak mildly shifting towards the right as v_{BL} increases. This implies that while BP2-4 are observable at BBO and DECIGO, BP1 is within the purview of LISA.

6 Conclusions

In this work, we have proposed a scale invariant version of the Zee-Babu model governed by an $U(1)_{B-L}$ gauge symmetry. The Zee-Babu framework also demands lepton number violation in the Lagrangian in order to address Majorana masses for the SM neutrinos, much like other seesaw scenarios. We argue that such a violation of a global $U(1)_L$ can be a consequence of a broken local $U(1)_{B-L}$. Anomaly cancellation necessitates including three RHNs which are chosen here to carry an \mathbb{Z}_2 charge so that

the lightest among them can be a potential DM candidate. The breaking of the $U(1)_{B-L}$ symmetry is catalysed by RG effects leading to a dynamically generated scale v_{BL} , which in turn triggers EWSB.

The crucial scalar trilinear coupling featuring in the minimal Zee-Babu set-up is now seen to get generated from a scalar quartic interaction via symmetry breaking. A key finding of this study is that the light neutrino mass scale is dictated by the symmetry breaking scale v_{BL} , given the classically scale invariant nature of the framework. In addition, LFV processes and the DM observables of relic density and direct detection cross section are also controlled by the same v_{BL} . We have adopted the Casas-Ibarra parameterisation to fit the neutrino oscillation data. Demanding that the lightest RHN alone accounts for the observed relic density and predicts an appropriately low DM-nucleon scattering rate constrains the symmetry breaking scale in the $10 \text{ TeV} \leq v_{BL} \leq 55 \text{ TeV}$ range.

We have also studied FOPTs in the aforementioned range by incorporating $T \neq 0$ corrections into the scalar potential. It is also demonstrated through representative parameter points that a *strong* FOPT can occur concomitantly with explaining the observed neutrino data and DM relic abundance while satisfying the bounds from LFV and DM direct detection. The corresponding stochastic GW spectra are mainly shaped by contributions from sound waves and bubble collisions, with the sound wave component generally dominating due to efficient energy transfer in relativistic fluids. We further report that GW spectra for the chosen parameter points can be probed using the future space-based detectors LISA and BBO.

Overall, an $U(1)_{B-L}$ -extended Zee-Babu model emerges as an attractive framework to test classical scale invariance through the window of neutrino mass and WIMP DM when the gauge symmetry is radiatively broken at an $\mathcal{O}(10 \text{ TeV})$ scale. Moreover, the model also leads to potentially detectable stochastic GW signatures.

Acknowledgements : UKD acknowledges support from the Anusandhan National Research Foundation (ANRF), Government of India under Grant Reference No. CRG/2023/003769.

Appendix

The one-loop β -functions for this model are given below.

$$\begin{aligned} 16\pi^2\beta_{\lambda_H} &= 24\lambda_H^2 + \lambda_1^2 + \lambda_2^2 + \lambda_3^2 - \lambda_H(3(g')^2 + 9g^2 - 12y_t^2) \\ &\quad + \frac{3}{8}(g')^4 + \frac{9}{8}g^4 + \frac{3}{4}(g')^2g^2 - 6y_t^4, \end{aligned} \quad (57a)$$

$$\begin{aligned} 16\pi^2\beta_{\lambda_h} &= 20\lambda_h^2 + 2\lambda_1^2 + \lambda_4^2 + \lambda_6^2 + 2\lambda_7^2 - \lambda_h(12(g')^2 + 48g_{BL}^2) \\ &\quad + 6(g')^4 + 48(g')^2g_{BL}^2 + 96g_{BL}^4, \end{aligned} \quad (57b)$$

$$\begin{aligned} 16\pi^2\beta_{\lambda_k} &= 20\lambda_k^2 + 2\lambda_2^2 + \lambda_5^2 + \lambda_6^2 - \lambda_k(48(g')^2 + 48g_{BL}^2) \\ &\quad + 96(g')^4 + 192(g')^2g_{BL}^2 + 96g_{BL}^4, \end{aligned} \quad (57c)$$

$$\begin{aligned} 16\pi^2\beta_{\lambda_S} &= 20\lambda_S^2 + 2\lambda_3^2 + \lambda_4^2 + \lambda_5^2 - \lambda_S(48g_{BL}^2 - 8\text{Tr}[Y_S^\dagger Y_S]) \\ &\quad + 96g_{BL}^4 - \text{Tr}[Y_S^\dagger Y_S Y_S^\dagger Y_S], \end{aligned} \quad (57d)$$

$$\begin{aligned} 16\pi^2\beta_{\lambda_1} &= 4\lambda_1^2 + 2\lambda_3\lambda_4 + 2\lambda_2\lambda_6 + 12\lambda_1\lambda_H + 8\lambda_1\lambda_h \\ &\quad - \lambda_1\left(\frac{15}{2}(g')^2 + \frac{9}{2}g^2 + 24g_{BL}^2 - 6y_t^2\right) + 3(g')^4, \end{aligned} \quad (57e)$$

$$\begin{aligned} 16\pi^2\beta_{\lambda_2} &= 4\lambda_2^2 + 2\lambda_3\lambda_5 + 2\lambda_1\lambda_6 + 12\lambda_2\lambda_H + 8\lambda_2\lambda_k \\ &\quad - \lambda_2\left(\frac{51}{2}(g')^2 + \frac{9}{2}g^2 + 24g_{BL}^2 - 6y_t^2\right) + 12(g')^4, \end{aligned} \quad (57f)$$

$$\begin{aligned} 16\pi^2\beta_{\lambda_3} &= 4\lambda_3^2 + 2\lambda_1\lambda_4 + 2\lambda_2\lambda_5 + 12\lambda_3\lambda_H + 8\lambda_3\lambda_S \\ &\quad - \lambda_3\left(\frac{3}{2}(g')^2 + \frac{9}{2}g^2 + 24g_{BL}^2 - 6y_t^2 - \text{Tr}[Y_S^\dagger Y_S]\right), \end{aligned} \quad (57g)$$

$$\begin{aligned} 16\pi^2\beta_{\lambda_4} &= 4\lambda_4^2 + 4\lambda_1\lambda_3 + 2\lambda_5\lambda_6 + 8\lambda_7^2 + 8\lambda_4\lambda_h + 8\lambda_4\lambda_S \\ &\quad - \lambda_4\left(6(g')^2 + 48g_{BL}^2 - \text{Tr}[Y_S^\dagger Y_S]\right) + 192g_{BL}^4, \end{aligned} \quad (57h)$$

$$\begin{aligned} 16\pi^2\beta_{\lambda_5} &= 4\lambda_5^2 + 4\lambda_2\lambda_3 + 2\lambda_4\lambda_6 + 4\lambda_7^2 + 8\lambda_5\lambda_k + 8\lambda_5\lambda_S \\ &\quad - \lambda_5\left(24(g')^2 + 48g_{BL}^2 - \text{Tr}[Y_S^\dagger Y_S]\right) + 192g_{BL}^4, \end{aligned} \quad (57i)$$

$$\begin{aligned} 16\pi^2\beta_{\lambda_6} &= 4\lambda_6^2 + 4\lambda_1\lambda_2 + 2\lambda_4\lambda_5 + 8\lambda_7^2 + 8\lambda_6\lambda_h + 8\lambda_6\lambda_k \\ &\quad - \lambda_6\left(30(g')^2 + 48g_{BL}^2\right) + 48(g')^4 + 192(g')^2g_{BL}^2 + 192(g')^4, \end{aligned} \quad (57j)$$

$$16\pi^2\beta_{\lambda_7} = \lambda_7\left(4\lambda_4 + 2\lambda_5 + 4\lambda_6 + 4\lambda_h - 12(g')^2 - 32g_{BL}^2 + \frac{1}{2}\text{Tr}[Y_S^\dagger Y_S]\right). \quad (57k)$$

$$16\pi^2\beta_{y_t} = y_t\left(\frac{9}{2}y_t^2 - \frac{17}{12}(g')^2 - \frac{9}{4}g^2 - 8g_s^2\right), \quad (58a)$$

$$16\pi^2\beta_{Y_S} = Y_S Y_S^\dagger Y_S + \frac{1}{2}Y_S \text{Tr}[Y_S^\dagger Y_S] - 6g_{BL}^2 Y_S. \quad (58b)$$

$$16\pi^2\beta_{g'} = \frac{17}{2}(g')^3, \quad (59a)$$

$$16\pi^2\beta_{g_{BL}} = \frac{44}{3}(g_{BL})^3, \quad (59b)$$

$$16\pi^2\beta_g = -\frac{19}{6}g^3, \quad (59c)$$

$$16\pi^2\beta_{g_s} = -7g_s^3. \quad (59d)$$

References

- [1] S. F. King, *Neutrino mass models*, *New J. Phys.* **6** (2004) 013, [[hep-ph/0310204](#)].
- [2] G. Altarelli and F. Feruglio, *Models of neutrino masses and mixings*, *New J. Phys.* **6** (2004) 106, [[hep-ph/0405048](#)].
- [3] R. N. Mohapatra and A. Y. Smirnov, *Neutrino mass and new physics*, *Ann. Rev. Nucl. Part. Sci.* **56** (2006) 569, [[hep-ph/0603118](#)].
- [4] M. C. Gonzalez-Garcia and M. Maltoni, *Phenomenology with massive neutrinos*, *Phys. Rept.* **460** (2008) 1, [[0704.1800](#)].
- [5] A. Zee, *Charged Scalar Field and Quantum Number Violations*, *Phys. Lett. B* **161** (1985) 141–145.

- [6] A. Zee, *Quantum Numbers of Majorana Neutrino Masses*, *Nucl. Phys. B* **264** (1986) 99–110.
- [7] K. S. Babu, *Model of 'Calculable' Majorana Neutrino Masses*, *Phys. Lett. B* **203** (1988) 132–136.
- [8] F. Zwicky, *Republication of: The redshift of extragalactic nebulae*, *General Relativity and Gravitation* **41** (Jan., 2009) 207–224.
- [9] V. C. Rubin and W. K. Ford, Jr., *Rotation of the Andromeda Nebula from a Spectroscopic Survey of Emission Regions*, *Astrophys. J.* **159** (1970) 379–403.
- [10] D. Clowe, M. Bradač, A. H. Gonzalez, M. Markevitch, S. W. Randall, C. Jones et al., *A direct empirical proof of the existence of dark matter*, *The Astrophysical Journal* **648** (Aug., 2006) L109–L113.
- [11] PLANCK collaboration, N. Aghanim et al., *Planck 2018 results. VI. Cosmological parameters*, *Astron. Astrophys.* **641** (2020) A6, [[1807.06209](#)].
- [12] F. S. Queiroz, *WIMP Theory Review*, *PoS EPS-HEP2017* (2017) 080, [[1711.02463](#)].
- [13] L. Roszkowski, E. M. Sessolo and S. Trojanowski, *WIMP dark matter candidates and searches—current status and future prospects*, *Rept. Prog. Phys.* **81** (2018) 066201, [[1707.06277](#)].
- [14] G. Arcadi, D. Cabo-Almeida, M. Dutra, P. Ghosh, M. Lindner, Y. Mambrini et al., *The Waning of the WIMP: Endgame?*, *Eur. Phys. J. C* **85** (2025) 152, [[2403.15860](#)].
- [15] E. Aprile, J. Aalbers, F. Agostini, M. Alfonsi et al., *First Dark Matter Search Results from the XENON1T Experiment*, *Phys. Rev. Lett.* **119** (2017) 181301, [[1705.06655](#)].
- [16] Z. Zhang et al., *Dark Matter Search Results from the PandaX-4T Experiment*, *Phys. Rev. Lett.* **129** (2022) 161804, [[2207.04828](#)].
- [17] D. S. Akerib et al., *First Dark Matter Search Results from the LUX-ZEPLIN (LZ) Experiment*, *Phys. Rev. Lett.* **131** (2023) 041002, [[2207.03764](#)].
- [18] U. K. Dey, S. K. Manna, P. K. Paul, S. K. Sahoo and N. Sahu, *Gravitational Wave Probe of Singlet-Doublet Dark Matter Induced Radiative Neutrino Mass*, [2511.19386](#).
- [19] I. K. Banerjee, U. K. Dey and S. Khalil, *Primordial Black Holes and Gravitational Waves in the $U(1)$ $B-L$ extended inert doublet model: a first-order phase transition perspective*, *JHEP* **12** (2024) 009, [[2406.12518](#)].
- [20] B. Fu, A. Ghoshal and S. F. King, *Cosmic string gravitational waves from global $U(1)_{B-L}$ symmetry breaking as a probe of the type I seesaw scale*, *JHEP* **11** (2023) 071, [[2306.07334](#)].
- [21] T. Hasegawa, N. Okada and O. Seto, *Gravitational waves from the minimal gauged $U(1)_{B-L}$ model*, *Phys. Rev. D* **99** (2019) 095039, [[1904.03020](#)].
- [22] T. Ohlsson, T. Schwetz and H. Zhang, *Non-standard neutrino interactions in the Zee-Babu model*, *Phys. Lett. B* **681** (2009) 269–275, [[0909.0455](#)].

[23] K. S. Babu, P. S. B. Dev, S. Jana and A. Thapa, *Non-Standard Interactions in Radiative Neutrino Mass Models*, *JHEP* **03** (2020) 006, [[1907.09498](#)].

[24] W. Chao, J.-H. Zhang and Y. Zhang, *Vacuum Stability and Higgs Diphoton Decay Rate in the Zee-Babu Model*, *JHEP* **06** (2013) 039, [[1212.6272](#)].

[25] E. J. Chun and S. Sharma, *Vacuum stability, perturbativity and scalar spectrum in the Zee-Babu model*, *Phys. Rev. D* **90** (2014) 035002, [[1406.5568](#)].

[26] S. Kanemura, M. Kikuchi and K. Yagyu, *Radiative corrections to the Higgs boson couplings in the Zee-Babu model*, *Phys. Rev. D* **90** (2014) 115018, [[1407.1336](#)].

[27] M. Nebot, J. F. Oliver, D. Palao and A. Santamaria, *Prospects for the Zee-Babu model at the CERN LHC and low energy experiments*, *Phys. Rev. D* **77** (2008) 093013, [[0711.0483](#)].

[28] D. Schmidt, T. Schwetz and H. Zhang, *Status of the Zee-Babu model for neutrino mass and possible tests at a like-sign linear collider*, *Nucl. Phys. B* **885** (2014) 524, [[1402.2251](#)].

[29] J. Herrero-Garcia, M. Nebot, N. Rius and A. Santamaria, *The Zee-Babu Model revisited in the light of new data*, *Nucl. Phys. B* **885** (2014) 542, [[1402.4491](#)].

[30] J. Herrero-Garcia, M. Nebot, N. Rius and A. Santamaria, *Testing the Zee-Babu model via neutrino data, lepton flavour violation and direct searches at the LHC*, *Nucl. Part. Phys. Proc.* **273-275** (2016) 1678, [[1410.2299](#)].

[31] M. Aoki, S. Kanemura and K. Yagyu, *Probing the Majorana nature of neutrinos in the Zee-Babu model at electron-positron colliders*, *Phys. Rev. D* **83** (2011) 075016, [[1108.1356](#)].

[32] E. J. Chun and S. Sharma, *Same-sign dilepton signals of the Zee-Babu model at lepton colliders*, *JHEP* **12** (2012) 107, [[1209.1303](#)].

[33] R. Ruiz, *Doubly Charged Higgs Boson Production at Hadron Colliders II: A Zee-Babu Case Study*, *JHEP* **10** (2022) 200, [[2206.14833](#)].

[34] A. Jueid, T. A. Chowdhury, S. Nasri and S. Saad, *Probing Zee-Babu states at Muon Colliders*, *Phys. Rev. D* **109** (2024) 075011, [[2306.01255](#)].

[35] A. Crivellin, M. Ghezzi, L. Panizzi, F. Piva et al., *Low- and high-energy phenomenology of a doubly charged scalar*, *Phys. Rev. D* **99** (2019) 035004, [[1807.10224](#)].

[36] T. B. de Melo, F. S. Queiroz and Y. Villamizar, *Doubly Charged Scalar at the High-Luminosity and High-Energy LHC*, *Int. J. Mod. Phys. A* **34** (2019) 1950157, [[1909.07429](#)].

[37] V. Q. Phong, N. C. Thao and H. N. Long, *Baryogenesis and gravitational waves in the Zee-Babu model*, *Eur. Phys. J. C* **82** (2022) 1005, [[2107.13823](#)].

[38] S.-L. Chen and Y.-Q. Xiao, *The neutrinoless double beta decay in the colored Zee-Babu model*, *Nucl. Phys. B* **986** (2023) 116041, [[2205.13118](#)].

[39] H. Okada and Y.-h. Qi, *Zee-Babu model in modular A_4 symmetry*, [2109.13779](#).

[40] T. Kobayashi, H. Okada and Y. Orikasa, *Zee-Babu model in a non-holomorphic modular A_4 symmetry and modular stabilization*, [2502.12662](#).

[41] K. S. Babu and S. Saad, *Ultraviolet completion of a two-loop neutrino mass model*, *JHEP* **03** (2025) 132, [[2412.14562](#)].

[42] N. Chakrabarty, C.-W. Chiang, T. Ohata and K. Tsumura, *Charged scalars confronting neutrino mass and muon $g - 2$ anomaly*, *JHEP* **12** (2018) 104, [[1807.08167](#)].

[43] R. Foot, A. Kobakhidze, K. L. McDonald and R. R. Volkas, *Neutrino mass in radiatively-broken scale-invariant models*, *Phys. Rev. D* **76** (2007) 075014, [[0706.1829](#)].

[44] S. Baek, *3.5 keV X-ray line signal from dark matter decay in local $U(1)_{B-L}$ extension of Zee-Babu model*, *JHEP* **08** (2015) 023, [[1410.1992](#)].

[45] K. L. McDonald and B. H. J. McKellar, *Evaluating the two loop diagram responsible for neutrino mass in Babu's model*, [hep-ph/0309270](#).

[46] J. A. Casas and A. Ibarra, *Oscillating neutrinos and $\mu \rightarrow e, \gamma$* , *Nucl. Phys. B* **618** (2001) 171–204, [[hep-ph/0103065](#)].

[47] I. Esteban, M. C. Gonzalez-Garcia, M. Maltoni, I. Martinez-Soler, J. P. Pinheiro and T. Schwetz, *NuFit-6.0: updated global analysis of three-flavor neutrino oscillations*, *JHEP* **12** (2024) 216, [[2410.05380](#)].

[48] J. Herrero-Garcia, M. Nebot, N. Rius and A. Santamaria, *The Zee–Babu model revisited in the light of new data*, *Nucl. Phys. B* **885** (2014) 542–570, [[1402.4491](#)].

[49] SINDRUM collaboration, U. Bellgardt et al., *Search for the Decay $\mu^+ \rightarrow e^+ e^+ e^-$* , *Nucl. Phys. B* **299** (1988) 1–6.

[50] MEG collaboration, A. M. Baldini et al., *Search for the lepton flavour violating decay $\mu^+ \rightarrow e^+ \gamma$ with the full dataset of the MEG experiment*, *Eur. Phys. J. C* **76** (2016) 434, [[1605.05081](#)].

[51] G. Cacciapaglia, C. Csaki, G. Marandella and A. Strumia, *The Minimal Set of Electroweak Precision Parameters*, *Phys. Rev. D* **74** (2006) 033011, [[hep-ph/0604111](#)].

[52] A. Semenov, *LanHEP: A Package for the automatic generation of Feynman rules in field theory. Version 3.0*, *Comput. Phys. Commun.* **180** (2009) 431–454, [[0805.0555](#)].

[53] G. Belanger, F. Boudjema, A. Pukhov and A. Semenov, *micrOMEGAs4.1: two dark matter candidates*, *Comput. Phys. Commun.* **192** (2015) 322–329, [[1407.6129](#)].

[54] P. B. Arnold and O. Espinosa, *The Effective potential and first order phase transitions: Beyond leading-order*, *Phys. Rev. D* **47** (1993) 3546, [[hep-ph/9212235](#)].

[55] A. D. Linde, *Decay of the false vacuum at finite temperature*, *Nuclear Physics B* **216** (1983) 421.

[56] A. I. Bochkarev, S. V. Kuzmin and M. E. Shaposhnikov, *On the Model Dependence of the Cosmological Upper Bound on the Higgs Boson and Top Quark Masses*, *Phys. Rev. D* **43** (1991) 369–374.

[57] M. Quiros, *Finite temperature field theory and phase transitions*, in *ICTP Summer School in High-Energy Physics and Cosmology*, pp. 187–259, 1, 1999. [hep-ph/9901312](#).

[58] J. M. Moreno, M. Quiros and M. Seco, *Bubbles in the supersymmetric standard model*, *Nucl. Phys. B* **526** (1998) 489–500, [[hep-ph/9801272](#)].

[59] L. D. McLerran, M. E. Shaposhnikov, N. Turok and M. B. Voloshin, *Why the baryon asymmetry of the universe is approximately 10^{*-10}* , *Phys. Lett. B* **256** (1991) 451–456.

[60] M. Dine, P. Huet and R. L. Singleton, Jr., *Baryogenesis at the electroweak scale*, *Nucl. Phys. B* **375** (1992) 625–648.

[61] F. C. Adams, *General solutions for tunneling of scalar fields with quartic potentials*, *Phys. Rev. D* **48** (1993) 2800–2805, [[hep-ph/9302321](#)].

[62] D. Bodeker and G. D. Moore, *Can electroweak bubble walls run away?*, *JCAP* **05** (2009) 009, [[0903.4099](#)].

[63] J. Ellis, M. Lewicki, J. M. No and V. Vaskonen, *Gravitational wave energy budget in strongly supercooled phase transitions*, *JCAP* **06** (2019) 024, [[1903.09642](#)].

[64] A. Roper Pol, S. Mandal, A. Brandenburg, T. Kahniashvili and A. Kosowsky, *Numerical simulations of gravitational waves from early-universe turbulence*, *Phys. Rev. D* **102** (2020) 083512, [[1903.08585](#)].

[65] T. Kahniashvili, A. Brandenburg, G. Gogoberidze, S. Mandal and A. Roper Pol, *Circular polarization of gravitational waves from early-Universe helical turbulence*, *Phys. Rev. Res.* **3** (2021) 013193, [[2011.05556](#)].

[66] A. Roper Pol, S. Mandal, A. Brandenburg and T. Kahniashvili, *Polarization of gravitational waves from helical MHD turbulent sources*, *JCAP* **04** (2022) 019, [[2107.05356](#)].

[67] P. Auclair, C. Caprini, D. Cutting, M. Hindmarsh, K. Rummukainen, D. A. Steer et al., *Generation of gravitational waves from freely decaying turbulence*, *JCAP* **09** (2022) 029, [[2205.02588](#)].

[68] C. Caprini et al., *Science with the space-based interferometer eLISA. II: Gravitational waves from cosmological phase transitions*, *JCAP* **04** (2016) 001, [[1512.06239](#)].

[69] J. Ellis, M. Lewicki, M. Merchand, J. M. No and M. Zych, *The scalar singlet extension of the Standard Model: gravitational waves versus baryogenesis*, *JHEP* **01** (2023) 093, [[2210.16305](#)].

[70] M. Lewicki, M. Merchand and M. Zych, *Electroweak bubble wall expansion: gravitational waves and baryogenesis in Standard Model-like thermal plasma*, *JHEP* **02** (2022) 017, [[2111.02393](#)].

[71] P. J. Steinhardt, *Relativistic Detonation Waves and Bubble Growth in False Vacuum Decay*, *Phys. Rev. D* **25** (1982) 2074.

[72] M. Kamionkowski, A. Kosowsky and M. S. Turner, *Gravitational radiation from first order phase transitions*, *Phys. Rev. D* **49** (1994) 2837–2851, [[astro-ph/9310044](#)].

[73] J. R. Espinosa, T. Konstandin, J. M. No and G. Servant, *Energy Budget of Cosmological First-order Phase Transitions*, *JCAP* **06** (2010) 028, [[1004.4187](#)].

[74] M. Hindmarsh, S. J. Huber, K. Rummukainen and D. J. Weir, *Gravitational waves from the sound of a first order phase transition*, *Phys. Rev. Lett.* **112** (2014) 041301, [[1304.2433](#)].

[75] M. Hindmarsh, S. J. Huber, K. Rummukainen and D. J. Weir, *Numerical simulations of acoustically generated gravitational waves at a first order phase transition*, *Phys. Rev. D* **92** (2015) 123009, [[1504.03291](#)].

[76] M. Hindmarsh, S. J. Huber, K. Rummukainen and D. J. Weir, *Shape of the acoustic gravitational wave power spectrum from a first order phase transition*, *Phys. Rev. D* **96** (2017) 103520, [[1704.05871](#)].

[77] M. B. Hindmarsh, M. Lüben, J. Lumma and M. Pauly, *Phase transitions in the early universe*, *SciPost Phys. Lect. Notes* **24** (2021) 1, [[2008.09136](#)].

[78] J. Ellis, M. Lewicki and J. M. No, *On the Maximal Strength of a First-Order Electroweak Phase Transition and its Gravitational Wave Signal*, *JCAP* **04** (2019) 003, [[1809.08242](#)].

[79] J. Ellis, M. Lewicki and J. M. No, *Gravitational waves from first-order cosmological phase transitions: lifetime of the sound wave source*, *JCAP* **07** (2020) 050, [[2003.07360](#)].

[80] H.-K. Guo, K. Sinha, D. Vagie and G. White, *Phase Transitions in an Expanding Universe: Stochastic Gravitational Waves in Standard and Non-Standard Histories*, *JCAP* **01** (2021) 001, [[2007.08537](#)].

[81] D. Cutting, M. Hindmarsh and D. J. Weir, *Gravitational waves from vacuum first-order phase transitions: from the envelope to the lattice*, *Phys. Rev. D* **97** (2018) 123513, [[1802.05712](#)].

[82] M. Lewicki and V. Vaskonen, *Gravitational waves from bubble collisions and fluid motion in strongly supercooled phase transitions*, *Eur. Phys. J. C* **83** (2023) 109, [[2208.11697](#)].

[83] LISA collaboration, P. Amaro-Seoane et al., *Laser Interferometer Space Antenna*, [1702.00786](#).

[84] G. M. Harry, P. Fritschel, D. A. Shaddock, W. Folkner and E. S. Phinney, *Laser interferometry for the big bang observer*, *Class. Quant. Grav.* **23** (2006) 4887–4894.

[85] S. Kawamura et al., *The Japanese space gravitational wave antenna: DECIGO*, *Class. Quant. Grav.* **28** (2011) 094011.

[86] W.-H. Ruan, Z.-K. Guo, R.-G. Cai and Y.-Z. Zhang, *Taiji program: Gravitational-wave sources*, *Int. J. Mod. Phys. A* **35** (2020) 2050075, [[1807.09495](#)].

[87] M. Punturo et al., *The Einstein Telescope: A third-generation gravitational wave observatory*, *Class. Quant. Grav.* **27** (2010) 194002.

[88] D. Reitze et al., *Cosmic Explorer: The U.S. Contribution to Gravitational-Wave Astronomy beyond LIGO*, *Bull. Am. Astron. Soc.* **51** (2019) 035, [[1907.04833](#)].

[89] LIGO SCIENTIFIC collaboration, J. Aasi et al., *Advanced LIGO*, *Class. Quant. Grav.* **32** (2015) 074001, [[1411.4547](#)].

[90] VIRGO collaboration, T. Accadia et al., *Virgo: a laser interferometer to detect gravitational waves*, *JINST* **7** (2012) P03012.

[91] KAGRA collaboration, K. Somiya, *Detector configuration of KAGRA: The Japanese cryogenic gravitational-wave detector*, *Class. Quant. Grav.* **29** (2012) 124007, [[1111.7185](#)].